

1 **Pattern- based Contractility Screening (PaCS), a reference-free traction force microscopy**  
2 **methodology, reveals contractile differences in breast cancer cells**

3 Ajinkya Ghagre, Ali Amini, Luv Kishore Srivastava, Pouria Tirgar, Adele Khavari, Newsha  
4 Koushki, Allen Ehrlicher\*

5 Department of Bioengineering, McGill University, Montreal, H3A 0E9

6 **Abstract**

7 The sensing and generation of cellular forces are essential aspects of life. Traction Force  
8 Microscopy (TFM) has emerged as a standard broadly applicable methodology to measure cell  
9 contractility and its role in cell behavior. While TFM platforms have enabled diverse discoveries,  
10 their implementation remains limited in part due to various constraints, such as time-consuming  
11 substrate fabrication techniques, the need to detach cells to measure null force images, followed  
12 by complex imaging and analysis, and the unavailability of cells for post-processing. Here we  
13 introduce a reference-free technique to measure cell contractile work in real-time, with basic  
14 substrate fabrication methodologies, simple imaging, and analysis with the availability of the cells  
15 for post-processing. In this technique, we confine the cells on fluorescent adhesive protein  
16 micropatterns of a known area on compliant silicone substrates and use the cell deformed pattern  
17 area to calculate cell contractile work. We validated this approach by comparing this Pattern-based  
18 Contractility Screening (PaCS) to conventional bead-displacement TFM and show quantitative  
19 agreement between the methodologies. Using this platform, we measure the contractile work of  
20 highly metastatic MDA-MB-231 breast cancer cells is significantly higher than non-invasive  
21 MCF-7 cells. PaCS enables the broader implementation of contractile work measurements in  
22 diverse quantitative biology and biomedical applications.

23 Keywords: Strain Energy, Contractility, Traction Force Microscopy, Micropatterning, Cancer  
24 metastasis

25 **Introduction**

26 Cells are not purely biochemical entities but are also subjected to physical forces and mechanics.  
27 Force-generation, sensing, and mechanical adaptation can be seen in nearly every aspect of our  
28 physiology<sup>1,2</sup>. Correct recognition of responses to mechanical cues are key to health, whereas  
29 dysfunctional responses are symptomatic and perhaps causative to numerous pathologies<sup>3-6</sup>. This  
30 signifies an urgent and pressing need to quantify how cells detect and respond to mechanical  
31 forces. This is a critical question in biology and biophysics, enabling new approaches in diagnosing  
32 and treating diverse aspects of human health.

33  
34 Cell contractile forces are largely generated by molecular motors such as myosin, which pull the  
35 filamentous actin network to perform mechanical work on the surrounding matrix<sup>7</sup>. There are  
36 diverse methodologies to measure cell contractile work<sup>8-10</sup>; however, Traction Force Microscopy  
37 (TFM) has emerged as the leading approach<sup>8-10</sup>. TFM has revealed the roles of cell contractile  
38 forces in regulating diverse physiological and pathological processes such as cell proliferation<sup>11</sup>,  
39 differentiation<sup>13</sup>, migration<sup>11,12</sup>, nuclear polarization and deformation<sup>15,16</sup>, in virtually all adherent

40 cells, thus making contractile work measurements a critical aspect of quantifying biological  
41 behaviors<sup>11-16</sup> and potentially identifying pathologies<sup>14</sup>.

42  
43 Although TFM is a widely useful technique, its implementation is limited in part due to  
44 experimental complexity<sup>8-10</sup>. TFM often utilizes protein functionalized elastic substrates, usually  
45 silicone or polyacrylamide, containing sub-micron fluorescent beads acting as fiduciary markers  
46 to capture cell-induced material deformations<sup>8</sup>. A typical TFM experiment involves imaging of the  
47 beads in the stressed state, followed by the detachment of cells to image the beads again to  
48 determine their positions in the unstressed state. The resulting two images are analyzed to calculate  
49 the total contractile work done by the cells in deforming the underlying substrate. Although TFM  
50 provides high-resolution traction force measurements due to the use of densely packed fluorescent  
51 beads, a limitation to this technique is lack of control over the placement and spacing of fiduciary  
52 markers<sup>9</sup>. These random bead arrangements necessitate the acquisition of a “null force” reference  
53 image to calculate the strain from cell-induced bead displacements, thus requiring cell detachment  
54 at the same position using enzymatic or chemical approaches<sup>9</sup>. This markedly complicates  
55 experimental procedures, imaging, and analysis, and precludes cellular post-processing, such as  
56 the immunofluorescence staining. While pillar-based approaches do not require a null-force image,  
57 they introduce topographical features that limit cell adhesion only to the pillar surface, thus  
58 affecting cell morphology, focal adhesions, cytoskeletal contractility, translocation of  
59 mechanosensitive proteins and stem cell differentiation<sup>23,24</sup>. Hence, there is a current void in cell  
60 contractility measurement methodologies that are readily implementable without affecting the  
61 biological features of the cells, thus limiting the incorporation of cell biophysics in modern  
62 quantitative biology studies.

63 Here, we introduce a novel reference-free approach to quantify cell contractile work based on the  
64 deformations of micropatterns of cell adhesion proteins. We print fibronectin micropatterns of  
65 known area and shape on compliant elastic silicone substrates; by imaging the cell-induced pattern  
66 area deformations and knowing substrate modulus, we calculate the total contractile work done by  
67 the cells to deform the patterns. The known pattern area makes it a reference-free approach,  
68 without introducing any specialized fabrication procedures or analysis. Continuous capture of  
69 pattern deformations allows real-time contractile measurements for longer periods of time with the  
70 ability to analyze a relatively large cell population without removing the cells, thus allowing cell  
71 post-processing of the same set of cells.

72

## 73 **Materials and Methods:**

### 74 **Synthesis of compliant silicone substrates**

75 To measure contractile work, polydimethylsiloxane (PDMS) substrates with different stiffnesses  
76 were prepared as described previously<sup>17,18,31</sup>. In brief, PDMS solutions were supplied by mixing  
77 same weight ratio of component A and B of commercial PDMS (NuSil® 8100, NuSil Silicone  
78 Technologies) with different concentrations of Sylgard 184 PDMS crosslinking agent (Dimethyl,  
79 methylhydrogen siloxane, which contains methyl terminated silicon hydride units) to obtain  
80 substrates with various stiffnesses. We measured the mechanical properties of the PDMS at  
81 different crosslinker concentrations using a parallel plate rheometer (Anton Paar) and calculated  
82 the Young's moduli (Table 1)<sup>17,18,31</sup>. For our experiments, 50  $\mu$ l of uncured PDMS was applied to

83 the clean 22\*22 mm (No.1) glass coverslips and cured at 100°C for two hours. For traction force  
84 microscopy, prepared PDMS substrates were coated with a layer of fiduciary particles using spin  
85 coater (WS-650 Spin Processor, Laurell Technologies) and incubated at 100 °C for an hour<sup>17,18</sup>.

86 **Table 1:** Young's moduli for PDMS substrates containing different concentrations of Sylgard 184 crosslinking  
87 agent<sup>17,18,31</sup>.

<b>Additional crosslinker concentration (weight %)</b>	<b>Young's modulus (YM) (kPa)</b>
0.00	0.3 ± 0.05
0.10	2.0 ± 0.06
0.20	5.0 ± 0.04
0.36	12.0 ± 0.71
0.50	23.4 ± 1.86
1.80	100.0 ± 2.80

88

89 Printing on silicone substrates using UV patterning.

90 We adhesively micropatterned silicone substrates with a UV-patterning system (PRIMO, Alveole  
91 Lab, Paris, France)<sup>19,20</sup>. PDMS substrates were incubated with Poly-L-Lysine (PLL, Sigma)  
92 solution (5mg/ml) prepared in 0.1M HEPES buffer (pH 8.5) for 1 hour at room temperature,  
93 followed by rinsing with MiliQ water. Positively charged PLL electrostatically adsorbs onto the  
94 negatively charged surface of silicone substrates and allows protein attachment after printing. The  
95 substrates were then incubated with Polyethylene glycol valeric acid (PEG-SVA, Laysan Bio)  
96 prepared in 0.1M HEPES buffer (pH 8.5) for 30 minutes at room temperature, followed by  
97 thorough rinsing with phosphate buffer saline (PBS) pH 7. PEG-SVA acts as an antifouling brush  
98 layer that repels protein attachment. The substrates were then covered with the UV sensitive photo-  
99 initiator solution of PLPP (Alveole Lab, Paris, France) and placed on the stage of a microscope  
100 (Nikon Ti2 Eclipse) equipped with the UV-patterning system.

101 To generate the patterns, we used open-source graphics software programs, Inkscape and ImageJ,  
102 to generate binary 8-bit mask image files that were loaded into PRIMO's control software. The  
103 desired pattern was generated by a digital micromirror array in the PRIMO system and projected  
104 using a 375 nm UV laser with an intensity of 29mW/mm<sup>2</sup> via 20X/0.45NA objective. The  
105 projected pattern results in localized photodegradation of the antifouling PEG-SVA brush, in the  
106 shape of the desired pattern. An exposure dose of 20 seconds was adequate to complete  
107 photodegradation of the PEG-SVA brush.

108 Following UV exposure, we washed the substrates with PBS and incubated them for 1 hr at room  
109 temperature with a mixture of fluorescently labeled bovine serum albumin (BSA, Alexa Fluor™  
110 555 conjugate, Thermofisher)(5µg/ml) and fibronectin (40µg/ml, Sigma) in PBS to adsorb the  
111 protein to the exposed PLL surface. Excess protein was rinsed off with PBS prior to cell seeding.

112

113

114

## 115 Cell culture and seeding

116 Cell lines used in this research: NIH-3T3 (ATCC-CRL1658) mouse fibroblast cells, MDA-MB-  
117 231 (ATCC-HTB-26) highly metastatic breast adenocarcinoma cells, MCF-7 (ATCC-HTB-22)  
118 low metastatic breast adenocarcinoma cells. All cell lines were cultured in Dulbecco's modified  
119 Eagle medium (DMEM) (Wisent) supplemented with 10% fetal bovine serum (FBS) (Wisent) and  
120 1% Penicillin-Streptomycin antibiotic (P/S) (Thermo Fisher). Cells were seeded on the patterns  
121 for 1 hour at 37°C in 5% CO<sub>2</sub> environment, followed by a gentle wash with PBS to remove  
122 nonattached cells to avoid nonspecific attachments. Cells were further incubated for 16-18 hours  
123 (on patterns) before imaging at 37°C in 5% CO<sub>2</sub> environment.

## 124 Imaging

125 After 16-18 hours of cell seeding, cells were stained with cell tracker green CMFDA  
126 (ThermoFisher) to detect cell boundaries, and the plates were transferred to a lab-built heated stage  
127 perfused with 5% CO<sub>2</sub> and mounted on a confocal microscope (Leica TCS SP8 with a 10x 0.4 NA  
128 objective). With this setup, cells were imaged with transmission and fluorescence microscopy for  
129 extended periods, while maintaining a controlled culture environment.

## 130 Immunofluorescence staining

131 For post-processing after contractile work measurements, we fixed the cells with 4%  
132 paraformaldehyde for 15 min at room temperature and washed three times with PBS. The cells  
133 were permeabilized with 0.1% Triton X-100 diluted in PBS for 10 minutes. To avoid any  
134 nonspecific hydrophobic binding, 2% bovine serum albumin (BSA) was added to the cells and  
135 incubated for 30 minutes at room temperature. After washing with PBS, we stained actin filaments  
136 with 10µg/ml Phalloidin (Alexa Fluor 647, ThermoFisher) for 1 hour at room temperature and  
137 nuclei with 1.5 µl/ml bisBenzimide H 33342 trihydrochloride (Sigma) for 10 minutes, after which  
138 cells were washed with PBS. Fluorescence images were acquired with a Leica SP8 confocal  
139 microscope with 63X/1.4 NA oil immersion objective.

## 140 Quantification of cell contractile work

141 To measure cell contractile work, we applied the following equation to calculate strain energy  
142 from pattern area deformations and material properties of the silicone substrates:

$$143 \quad U = 2GA_f t \left(1 - \frac{A_f}{A_i}\right)$$

144 Where  $U$ ,  $A_i$ ,  $A_f$ ,  $G$  and  $t$  are total strain energy, initial pattern area, deformed pattern area,  
145 substrate shear modulus and substrate thickness respectively (derivation in Supporting Material).  
146 In brief, we measure the deformed and undeformed pattern area by thresholding the fluorescent  
147 pattern images. For strain energy calculations, we use a single averaged value of undeformed  
148 pattern area ( $2401.96 \pm 32.24 \mu\text{m}^2$ , Fig S1a) and compare it with the cell deformed pattern area,  
149 which along with known modulus of silicone substrate allows us to calculate total strain energy  
150 applied by the cells to deform the underlying substrate. We calculate outlier strain energy values  
151 from undeformed pattern areas on each stiffness substrates (Fig S1b).

152 Data analysis

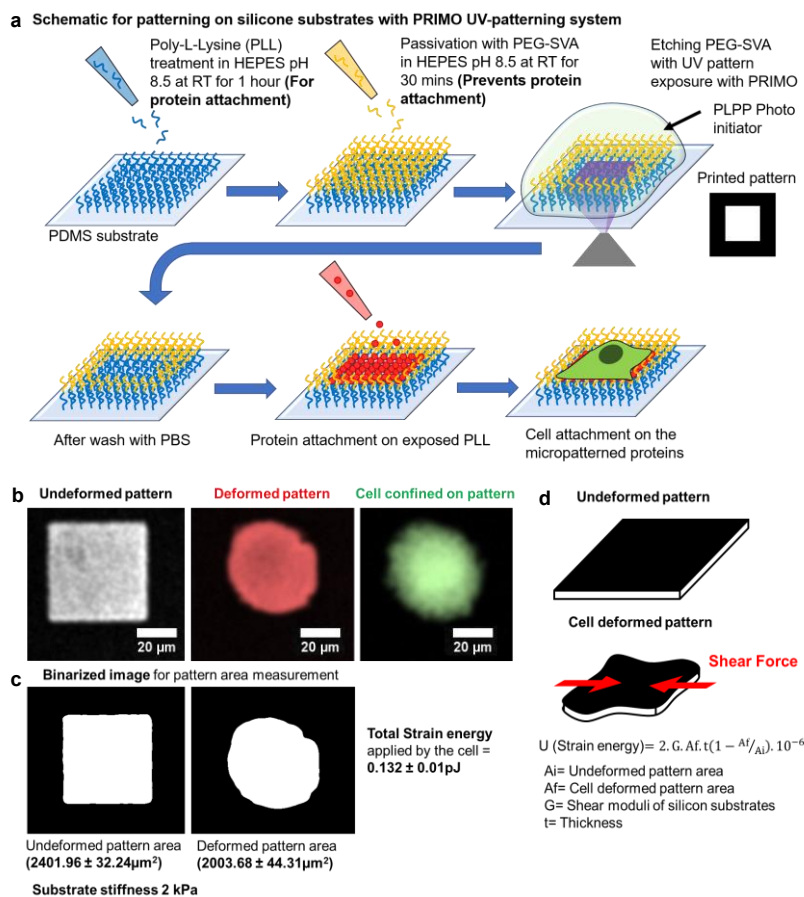
153 Cell strain energy was calculated using a custom MATLAB script which requires fluorescent  
154 pattern images, substrate stiffness and initial pattern area. The code calculates the pattern area and  
155 strain energy values for the respective cells. The code is available on the GitHub repository with  
156 experimental details and example data for analysis ([https://github.com/ajinkyaghagre/PaCS\\_](https://github.com/ajinkyaghagre/PaCS_matlabcode)  
157 [matlabcode](https://github.com/ajinkyaghagre/PaCS_matlabcode)). Further relevant data are available from corresponding authors request.

158

159 **Results:**

160 **PaCS Design and Analysis**

161 In PaCS, adhesive protein micropatterns are printed on the surface of compliant silicone substrates.  
162 We chose polydimethylsiloxane (PDMS) because of its favorable material properties such as the  
163 ability to tune its stiffness over a large physiological range, chemical stability (nondegradable) and  
164 bioinertness<sup>17,18</sup>. PDMS is also optically transparent (refractive index ~1.4) and amenable to spin  
165 coating. This facilitates creating a uniform and flat surface that avoids the confounding effects of  
166 hydrogel porosity on the cells<sup>17,18</sup>.



167

168

169 **Figure 1: Cells deform adhesive protein patterns on compliant silicone substrates:** **a**, Schematic for patterning  
 170 on silicone substrates with PRIMO photopatterning system. **b**, Fluorescent BSA and fibronectin square pattern on 2  
 171 kPa PDMS substrates undeformed (white) and deformed by the cell (red). Cell on the pattern stained with CMFDA  
 172 cell tracker (green). **c**, Binarized image of the undeformed and deformed pattern used for area measurements, used to  
 173 calculate total strain energy applied by the cells to deform the underlying pattern, in this case  $0.132 \pm 0.01$  pJ. **d**,  
 174 Schematic explanation for strain energy calculations using the volumetric strain approach.

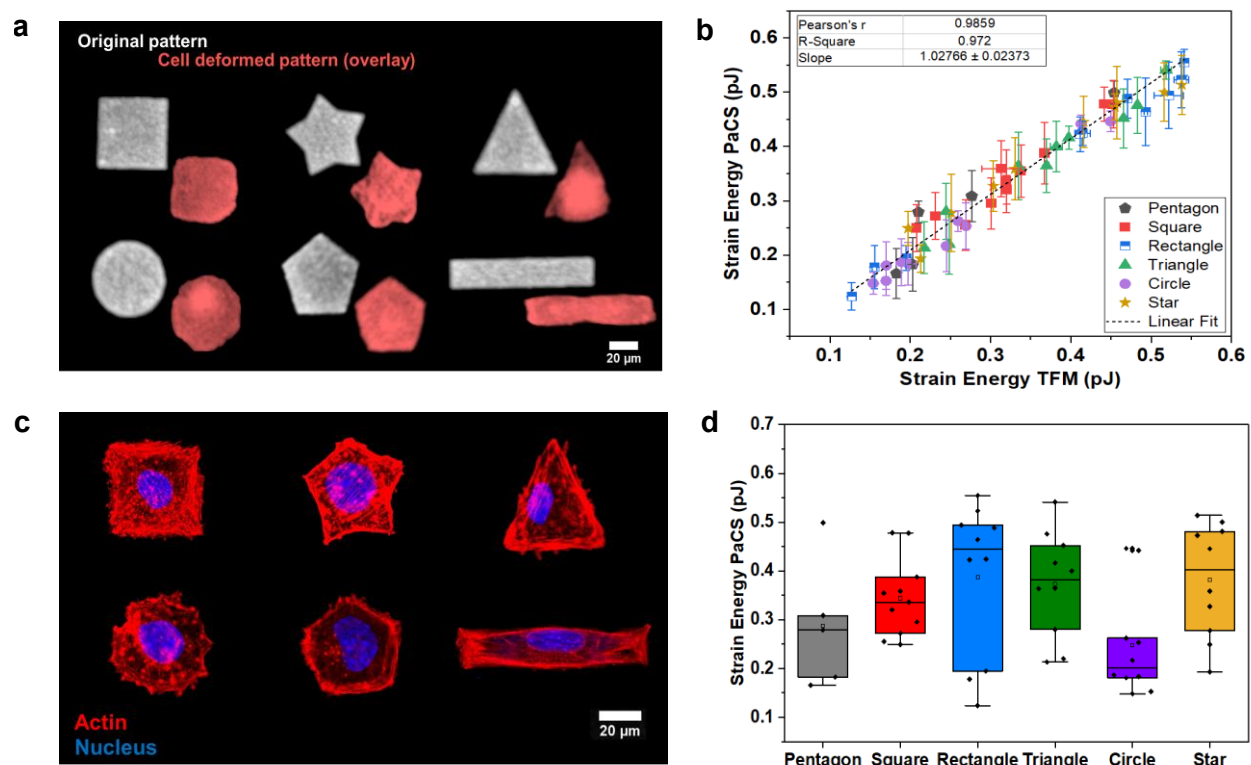
175 We cured flat PDMS substrates of specific Young's moduli ( $E = 2 \pm 0.06$ ,  $12 \pm 0.71$  and  $23.45 \pm$   
 176  $1.86$  kPa) on cover glass as described previously<sup>17,18</sup>. Next, we printed adhesive protein  
 177 micropatterns of desired shapes and sizes on PDMS substrates using the PRIMO photopatterning  
 178 system<sup>19,20</sup>.

179 In brief, the PDMS substrates were first coated with PLL which promotes cell attachment,  
 180 followed by a coating with an antifouling agent PEG-SVA. The PRIMO photopatterning system  
 181 utilizes a UV laser which projects the desired pattern on the surface of the PDMS substrates. The  
 182 projected UV laser etches PEG-SVA in the presence of a photo initiator PLPP, thus exposing the  
 183 underlying PLL layer for adhesive protein attachment (Fig 1a). Using this system, we confined  
 184 NIH 3T3 fibroblast cells on square micropatterns of  $\sim 2400 \mu\text{m}^2$  printed on 2 kPa PDMS substrates  
 185 (Fig 1b). We used a combination of fluorescent BSA and fibronectin for pattern visualization and  
 186 cell attachment. Fibroblast cells deform the soft silicone substrate using contractile forces thus



187 deforming the printed patterns into arbitrary shapes (Fig 1b). We binarize the images to measure  
188 the deformed pattern area and compare it with the initial pattern area (Fig 1c), which along with  
189 material properties of silicone allows us to calculate total contractile work done (strain energy) by  
190 the cell to deform the substrate (Fig 1d, Supporting Material). In this case, the representative  
191 fibroblast cell is applying a strain energy of  $0.132 \pm 0.01$  pJ, deforming the square pattern of  
192  $2401.96 \pm 32.24 \mu\text{m}^2$  to a pattern area of  $2003.68 \pm 44.31 \mu\text{m}^2$ , on a 2 kPa PDMS substrate (Fig  
193 1b, c).

194 **PaCS accurately captures contractile work across diverse cell shapes.**



195  
196 **Figure 2: PaCS accurately measures cell contractile work across diverse cell shapes:** **a**, Fluorescent BSA-  
197 fibronectin patterns of various shapes deformed by 3T3 Fibroblast cells on 12 kPa PDMS substrates. **b**, Total strain  
198 energy calculated with PaCS strongly correlates with strain energy calculated with TFM ( $n=56$ ). **c**, 3T3 Fibroblast  
199 cells fixed and stained with phalloidin (actin) and DAPI (nuclei), imaged on Leica SP8 confocal (63X/1.4NA  
200 objective). **d**, PaCS strain energy for 3T3 Fibroblast cells indicate cells confined in circular shape to apply the least  
201 strain energy.

202 To determine the accuracy of our contractile work measurement, we measured cell strain energy  
203 using both conventional bead-based TFM and PaCS simultaneously. We coated the PDMS  
204 substrates with fluorescent beads, followed with printing of adhesive micropatterns on the  
205 substrates. Fluorescent beads allow us to measure contractile work with bead-displacement TFM  
206 and compare it with the contractile work calculated from PaCS for the same cells. We printed  
207 micropatterns of the same area ( $\sim 2400 \mu\text{m}^2$ ) but with different shapes (square, circle, triangle,  
208 rectangle, star, and pentagon) on PDMS substrates with a Young's modulus of 12 kPa and

209 measured cell contractile work of NIH 3T3 fibroblast cells with both bead-displacement TFM and  
210 PaCS.

211 Fibroblast cells confined on diverse pattern shapes deformed the patterns, the areas of which were  
212 used to quantify cell contractile work (Fig 2a, S2a). When compared with bead-based TFM  
213 measurements, PaCS accurately measured contractile work of fibroblast cells confined on patterns  
214 of all investigated different shapes (Fig 2b). The increased pattern deformations strongly correlate  
215 with higher strain energies applied by the cells to deform the underlying substrate (Fig S2b). Thus,  
216 PaCS accurately and precisely measures cell contractile work irrespective of pattern shape with  
217 the availability of the cells for post processing.

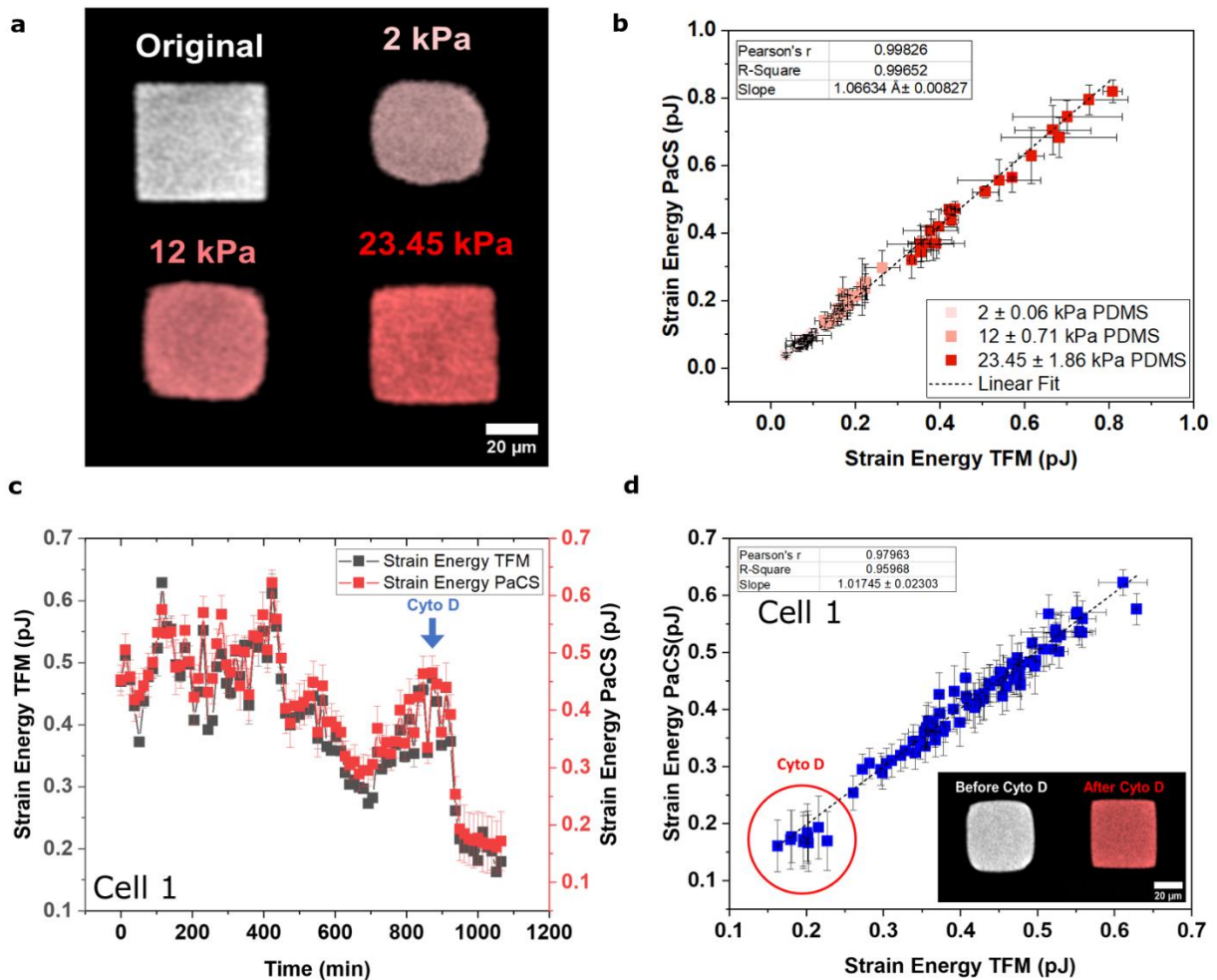
218 To demonstrate the ability of this technique to allow post-processing, we fixed and stained the  
219 confined cells with phalloidin and DAPI to visualize the actin filaments and nucleus, respectively  
220 (Fig 2c). Consistent with previous work<sup>27-30</sup>, these fluorescent images reveal that actin filaments  
221 are most concentrated on external polygon edges and terminate at polygon vertices. Conversely,  
222 circular shapes appear to promote radially aligned actin filaments in the cell, which results in cell  
223 applying lower strain energies when compared with other cell shapes (Fig 2d). These data show  
224 how profoundly cell geometry impacts cytoskeletal structure.

### 225 **PaCS resolves time-dependent contractile work and cytoskeletal activity as a function of** 226 **substrate stiffness.**

227 To examine the accuracy of PaCS on different moduli substrates, as before we compared PaCS  
228 measurements with bead-based TFM using PDMS substrates coated with fluorescent beads. We  
229 measured the contractile work of 3T3 fibroblast cells on square patterns of the same area  
230 ( $\sim 2400\mu\text{m}^2$ ) printed on PDMS substrates with Young's moduli of 2, 12 and 23.45 kPa. We  
231 observed decreased pattern deformation with increasing substrate stiffness (Fig 3a, S3b), and that  
232 cells applied more contractile work on stiffer substrates (Fig 3b). The contractile work  
233 measurements from PaCS are highly correlated with the work calculated with TFM (Fig 3b). Thus,  
234 PaCS accurately and precisely resolved contractile differences of cells on different stiffness PDMS  
235 substrates (Fig S3c).

236 We further tested the ability of PaCS to resolve time-dependent contractile work. We measured  
237 fibroblast cell contractile work on square patterns ( $\sim 2400\mu\text{m}^2$ ) on PDMS substrates (12 kPa) for  
238 18 hours; to further test the sensitivity of this technique we inhibited the cell contractile work by  
239 depolymerizing actin using Cytochalasin D (Cyto D) in the last few hours of measurement. Using  
240 time-dependent PaCS, we accurately measured cell contractile work with time when compared to  
241 TFM measurements, even after the Cyto D treatment (Fig 3c and d, S4). The increased pattern area  
242 after drug treatment, indicates decreased contractile work of the cell with time. (Fig 3d, inset, S4)





243

244 **Figure 3: PaCS resolves time dependent contractile work and cytoskeletal activity as a function of substrate**  
 245 **stiffness.** **a**, Pattern deformations by 3T3 fibroblast cells on PDMS substrates of different Young's moduli (2, 12 and  
 246 23.45 kPa) **b**, Total strain energy calculated with pattern deformations strongly correlates with strain energy calculated  
 247 with TFM (n=60). **c**, Time-dependent relation between strain energy calculated with PaCS and TFM (cell 1), blue  
 248 arrow represents the time of addition of Cyto D (Time interval 12.83mins) (n=84 timepoints). **d**, Strain energy  
 249 calculated with pattern deformations with time strongly correlates with strain energy calculated with TFM, red circle  
 250 represents the strain energy values after Cyto D (n=84 timepoints).

251 Hence, PaCS accurately and precisely measures time-dependent contractile work as a function of  
 252 substrate stiffness, without the need for a null force image, thereby enabling higher number of  
 253 measurements per experiment, with the availability of the cells for post-processing such as  
 254 immunofluorescence.

255

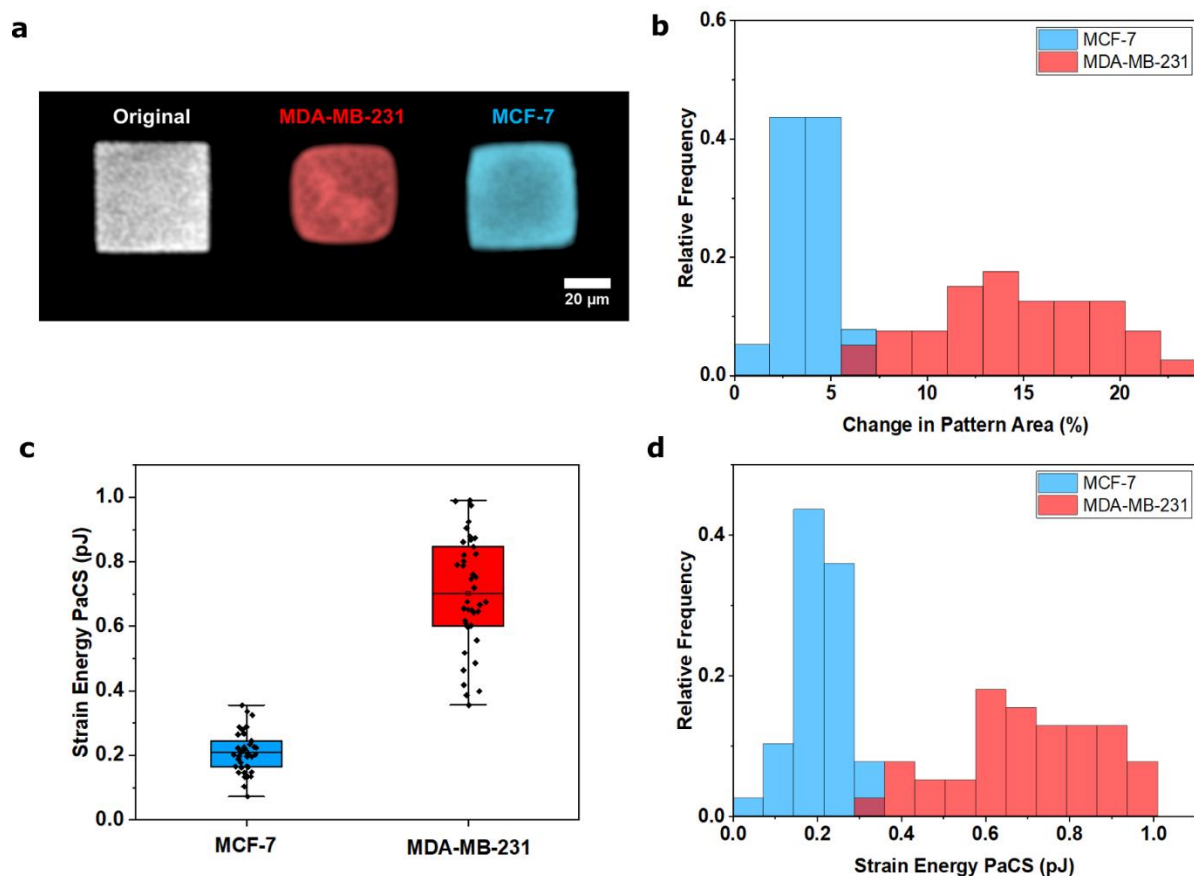
256

257

258

259 **PaCS reveals contractile work differences between metastatic breast cancer cells.**

260 To exemplify potential applications of this technique, we performed contractile work  
261 measurements using PaCS on low and highly metastatic breast cancer cells. The tumor  
262 microenvironment undergoes diverse mechanical and chemical changes throughout the neoplastic  
263 progression<sup>21,22</sup>. During cancer metastasis, cells from the primary tumor site acquire the ability to  
264 escape and migrate through the heterogeneous tumor microenvironment to establish secondary  
265 tumors. Despite being linked to poor prognosis, there are few direct biophysical clinical tests  
266 available to diagnose the likelihood of metastasis<sup>21,22</sup>. Because metastasis of most solid tumors  
267 requires cells to exert force to reorganize and navigate through the dense stroma, and has been  
268 previously correlated with contractility<sup>21,22</sup>, we investigated the differences in cellular force  
269 generation between low and highly metastatic cancer cells with PaCS. In this study we measured  
270 contractile work of highly metastatic (MDA-MB231) and weakly metastatic (MCF-7) breast  
271 cancer cells using square patterns ( $\sim 2400\mu\text{m}^2$ ) printed on 12 kPa PDMS substrates. Highly  
272 metastatic MDA-MB-231 cells exhibited higher pattern deformation than low metastatic MCF-7  
273 cells (Fig 5a, b and S5). In agreement with previous findings, we observed that highly metastatic  
274 cancer cells exerted larger strain energies than breast cancer cells with lower metastatic potential  
275 (Fig 5c, d)<sup>21</sup>. These results demonstrate the ability of PaCS to resolve contractile changes between  
276 different cancer cell types, which may lead to simplified biophysical clinical tests to diagnose  
277 cancer metastasis.



278

279 **Figure 4: PaCS reveals contractile differences between low metastatic and highly metastatic breast cancer cells.**

280 **a**, Pattern deformations for high metastatic MDA-MB-231 (red) and low metastatic MCF-7 (blue) cells, show higher  
281 deformations by highly metastatic cells. **b**, Histogram of percent change in pattern area for MDA-MB-231 (n=40) and  
282 MCF-7 cells (n=39). **c**, PaCS Strain Energy for MDA-MB-231 cells (n=40) and MCF-7 cells (n=39). **d**, Histogram of  
283 strain energy for MDA-MB-231 cells (n=40) and MCF-7 cells (n=39) reveal contractile differences between the cell  
284 lines, with highly metastatic cell being more contractile.

285

## 286 Discussion

287 PaCS combines the approaches of adhesive protein micropatterning on soft silicone materials with  
288 automated image analysis to provide real-time cell contractile work measurements. The soft  
289 silicone base offers tunable stiffness in physiological range<sup>17,18</sup>, along with controlled cell  
290 confinement using adhesive protein micropatterns, broadens its applications across multiple cell  
291 types and functions.

292 We demonstrate the ability of PaCS to measure cell contractile work of fibroblast cells across  
293 diverse shapes and highlight its potential to resolve increasing contractile work of cells on  
294 increasing substrate stiffness. The correlation with conventional TFM revealed high accuracy of  
295 PaCS in measuring contractile work across all diverse shapes and substrate stiffness.

296 Although conventional TFM and micropillar techniques provide multi-dimensional force  
297 resolutions in the form of vectors assigned to specific focal adhesions, such techniques are limited  
298 to specific biophysical questions for a limited number of cells<sup>8-10,26,27</sup>. Such techniques require  
299 high resolution imaging to resolve small scale forces and demands extensive workflow, which  
300 comes at a cost of the limited number of measurements and simplicity. PaCS is a reference-free  
301 platform, that measures contractile work from a single image of deformed patterns, thus  
302 simplifying the experimental workflow and increasing the number of measurements per  
303 experiment.

304 The use of unconfined cells in TFM and micropillar techniques further complicates the workflow  
305 with the requirement of precise position monitoring of the cells moving within each time frame.  
306 In PaCS cells are restricted to a single position and do not migrate which simplifies further imaging  
307 and analysis. Time-dependent PaCS measurements of fibroblast cells on silicone substrates,  
308 revealed a strong correlation of contractile work with TFM, and highlighted the time-dependent  
309 sensitivity of the technique after treatment with contractile inhibitor.

310 Moreover, micropillar and microdot techniques complicate the measurements by introducing  
311 additional topographical features on the substrate surface, along with variations in distance  
312 between the dots or pillars, all of which have shown to affect the biology of the cells<sup>23,24</sup>. In PaCS  
313 cells are on confined adhesive patterns on continuous substrates, thus avoiding any effect from  
314 topographical features of the substrate.

315 We further demonstrate a potential application of PaCS in resolving contractile work differences  
316 in cancer cells. During cancer metastasis, the neoplastic microenvironment not only confers  
317 biochemical changes but also alters the biophysical phenotype of cancer cells<sup>25</sup>. Malignant cells  
318 are reported to be highly contractile with increased migration and compliance. Such biophysical  
319 markers can be used to diagnose metastatic potential of cancer cells or can be screened to develop  
320 treatments that directly target these biophysical characteristics and thus effectively hinder  
321 metastasis. Contractile forces are emerging as biophysical markers in the majority of cancer  
322 models including breast, prostate, lung and bone<sup>21,25</sup>.

323 In this study we used PaCS to measure contractile work differences between highly metastatic  
324 (MDA-MB-231) and weakly metastatic (MCF-7) breast cancer cells. In agreement with the  
325 previous finding, PaCS detects high contractile work done by invasive MDA-MB-231 breast  
326 cancer cells, when compared to less invasive MCF-7 cells, thus highlighting the involvement of  
327 contractility in cancer metastatic progression. The ability of PaCS to detect contractile work  
328 differences across multiple cell types, broadens the horizon of its applications.

329 Recently contractile forces have been implemented as a crucial parameter for anti-cancer and  
330 bronchoconstrictor drug screenings, thus demonstrating the potential of PaCS for drug screening  
331 applications<sup>22,26</sup>. With further advancements PaCS has the potential to become a leading  
332 technology for the diagnosis of diseased conditions involving aberrant cellular force generation.

333 PaCS can be used to study the physiological role of contractile forces in regulating biological  
334 processes such as cell migration, proliferation, stem cell differentiation and nuclear deformation.  
335 Such studies need to be explored further to understand the complexity of cell biological processes.

336 However, such widespread use of cell mechanics across cell biology and medicine is limited by  
337 the inadaptability of current approaches across multiple labs. The standard techniques such as TFM  
338 are too difficult too be operated by non-experts, thus creating a demand for simple adaptable  
339 techniques that can be operated by anyone. PaCS provides a quick and accurate contractile work  
340 measurement with a simple workflow, which makes it readily adaptable across multiple labs.  
341 While we have demonstrated this approach using UV micropatterning, we anticipate that broader  
342 implementation could also be achieved with soft-lithography based microcontact printing<sup>32</sup>.

### 343 **Conclusion**

344 In this paper we introduce a new technique to measure cell contractile work using adhesive pattern  
345 deformations. This technique allows for real-time cell contractile measurements with simpler  
346 fabrication protocols and analysis. Using this technique, we revealed contractile work differences  
347 of fibroblast cells confined on different shapes and substrate stiffness. We measured differences  
348 in contractile work with the time and observed the differences after drug-induced contractile  
349 inhibition. Finally, we demonstrate the application of this technique in resolving the contractile  
350 work differences in benign and metastatic breast cancer cells. The ability of this technique to  
351 measure contractile work in real-time from the pattern deformations fills a current void in  
352 simplified cell contractile methodologies, and provides a promising future for the incorporation of  
353 cell biophysics in broader quantitative biology studies.

### 354 **Acknowledgements:**

355 AJE acknowledges grant support from NSERC (RGPIN/05843-2014, EQPEQ/472339-2015,  
356 RTI/00348-2018), Canadian Cancer Society Grant #703930, Canadian Foundation for Innovation  
357 Project #32749, Prostate Cancer Canada D2019-2180, the Canada Research Chairs program, and  
358 CIHR # 143327. AG, AA, LKS, PT, NK were partially supported by McGill Engineering doctoral  
359 awards. The authors thank Dr Peter Seigel for the kind gifts of breast cancer cell lines MDA-MB-  
360 231 (ATCC-HTB-26) highly metastatic breast adenocarcinoma cells, MCF-7 (ATCC-HTB-22)  
361 low metastatic breast adenocarcinoma cells.

362

363

364

365

366

367

368

369

370

371

372 **References:**

- 373 1. Vogel, V. & Sheetz, M. Local force and geometry sensing regulate cell functions. *Nat. Rev.*  
374 *Mol. Cell Biol.* **7**, 265–75 (2006).
- 375 2. Wang, N., Tytell, J. D. & Ingber, D. E. Mechanotransduction at a distance: mechanically  
376 coupling the extracellular matrix with the nucleus. *Nat Rev Mol Cell Biol* **10**, 75–82 (2009).
- 377 3. Discher, D. E. The foldome in cellular force transduction. *Conf Proc IEEE Eng Med Biol*  
378 *Soc* **1**, 3341–3342 (2009).
- 379 4. Hahn, C. & Schwartz, M. A. The role of cellular adaptation to mechanical forces in  
380 atherosclerosis. *Arter. Thromb Vasc Biol* **28**, 2101–2107 (2008).
- 381 5. Jaalouk, D. E. & Lammerding, J. Mechanotransduction gone awry. *Nat. Rev. Mol. Cell*  
382 *Biol.* **10**, 63–73 (2009).
- 383 6. Ingber, D. E. Mechanobiology and diseases of mechanotransduction. *Ann Med* **35**, 564–  
384 577 (2003).
- 385 7. Murrell, M., Oakes, P., Lenz, M. and Gardel, M., 2015. Forcing cells into shape: the  
386 mechanics of actomyosin contractility. *Nature Reviews Molecular Cell Biology* **16**, pp.486-  
387 498.
- 388 8. Polacheck, W. and Chen, C., 2016. Measuring cell-generated forces: a guide to the  
389 available tools. *Nature Methods* **13**, pp.415-423.
- 390 9. Banda, O., Sabanayagam, C. and Slater, J., 2019. Reference-Free Traction Force  
391 Microscopy Platform Fabricated via Two-Photon Laser Scanning Lithography Enables  
392 Facile Measurement of Cell-Generated Forces. *ACS Applied Materials & Interfaces*,  
393 **11(20)**, pp.18233-18241.
- 394 10. Bergert, M., Lendenmann, T., Zündel, M., Ehret, A., Panozzo, D., Richner, P., Kim, D.,  
395 Kress, S., Norris, D., Sorkine-Hornung, O., Mazza, E., Poulidakos, D. and Ferrari, A.,  
396 2016. Confocal reference free traction force microscopy. *Nature Communications*, **7(1)**.
- 397 11. Martino, F., Perestrelo, A., Vinarský, V., Pagliari, S. and Forte, G., 2018. Cellular  
398 Mechanotransduction: From Tension to Function. *Frontiers in Physiology*, **9**.
- 399 12. Wolfenson, H., Yang, B. and Sheetz, M., 2019. Steps in Mechanotransduction Pathways  
400 that Control Cell Morphology. *Annual Review of Physiology*, **81(1)**, pp.585-605.
- 401 13. Sun, Y., Chen, C. and Fu, J., 2012. Forcing Stem Cells to Behave: A Biophysical  
402 Perspective of the Cellular Microenvironment. *Annual Review of Biophysics*, **41(1)**,  
403 pp.519-542.
- 404 14. Przybyla, L., Muncie, J. and Weaver, V., 2016. Mechanical Control of Epithelial-to-  
405 Mesenchymal Transitions in Development and Cancer. *Annual Review of Cell and*  
406 *Developmental Biology*, **32(1)**, pp.527-554.
- 407 15. Versaevel, M., Grevesse, T. and Gabriele, S., 2012. Spatial coordination between cell and  
408 nuclear shape within micropatterned endothelial cells. *Nature Communications*, **3(1)**.
- 409 16. Li, Q., Makhija, E., Hameed, F. and Shivashankar, G., 2015. Micropillar displacements by  
410 cell traction forces are mechanically correlated with nuclear dynamics. *Biochemical and*  
411 *Biophysical Research Communications*, **461(2)**, pp.372-377.
- 412 17. Yoshie, H., Koushki, N., Kaviani, R., Tabatabaei, M., Rajendran, K., Dang, Q., Husain,  
413 A., Yao, S., Li, C., Sullivan, J., Saint-Geniez, M., Krishnan, R. and Ehrlicher, A., 2018.  
414 Traction Force Screening Enabled by Compliant PDMS Elastomers. *Biophysical Journal*,



- 415 **114(9)**, pp.2194-2199.
- 416 18. Yoshie, H., Koushki, N., Molter, C., Siegel, P.M., Krishnan, R. and Ehrlicher, A.J., 2019.
- 417 High Throughput Traction Force Microscopy Using PDMS Reveals Dose-Dependent
- 418 Effects of Transforming Growth Factor- $\beta$  on the Epithelial-to-Mesenchymal Transition.
- 419 *JoVE (Journal of Visualized Experiments)*, **(148)**, p.e59364.
- 420 19. Polio, S.R., Stasiak, S.E., Jamieson, R.R., Balestrini, J.L., Krishnan, R. and Parameswaran,
- 421 H., 2019. Extracellular matrix stiffness regulates human airway smooth muscle contraction
- 422 by altering the cell-cell coupling. *Scientific reports*, **9(1)**, pp.1-12.
- 423 20. Toro-Nahuelpan, M., Zagoriy, I., Senger, F., Blanchoin, L., Théry, M. and Mahamid, J.,
- 424 2020. Tailoring cryo-electron microscopy grids by photo-micropatterning for in-cell
- 425 structural studies. *Nature Methods*, **17(1)**, pp.50-54.
- 426 21. Kraning-Rush, C.M., Califano, J.P. and Reinhart-King, C.A., 2012. Cellular traction
- 427 stresses increase with increasing metastatic potential. *PloS one*, **7(2)**.
- 428 22. Li, Z., Persson, H., Adolfsson, K., Abariute, L., Borgström, M.T., Hessman, D., Åström,
- 429 K., Oredsson, S. and Prinz, C.N., 2017. Cellular traction forces: a useful parameter in
- 430 cancer research. *Nanoscale*, **9(48)**, pp.19039-19044.
- 431 23. Wang, X., Hu, X., Dulińska-Molak, I., Kawazoe, N., Yang, Y. and Chen, G., 2016.
- 432 Discriminating the Independent Influence of Cell Adhesion and Spreading Area on Stem
- 433 Cell Fate Determination Using Micropatterned Surfaces. *Scientific Reports*, **6(1)**.
- 434 24. Fu, J., Wang, Y., Yang, M., Desai, R., Yu, X., Liu, Z. and Chen, C., 2010. Mechanical
- 435 regulation of cell function with geometrically modulated elastomeric substrates. *Nature*
- 436 *Methods*, **7(9)**, pp.733-736.
- 437 25. Holenstein, C., Horvath, A., Schär, B., Schoenenberger, A., Bollhalder, M., Goedecke, N.,
- 438 Bartalena, G., Otto, O., Herbig, M., Guck, J., Müller, D., Snedeker, J. and Silvan, U., 2019.
- 439 The relationship between metastatic potential and in vitro mechanical properties of
- 440 osteosarcoma cells. *Molecular Biology of the Cell*, **30(7)**, pp.887-898.
- 441 26. Pushkarsky, I., Tseng, P., Black, D., France, B., Warfe, L., Koziol-White, C., Jester, W.,
- 442 Trinh, R., Lin, J., Scumpia, P., Morrison, S., Panettieri, R., Damoiseaux, R. and Di Carlo,
- 443 D., 2018. Elastomeric sensor surfaces for high-throughput single-cell force cytometry.
- 444 *Nature Biomedical Engineering*, **2(2)**, pp.124-137.
- 445 27. Kilian, K., Bugarija, B., Lahn, B. and Mrksich, M., 2010. Geometric cues for directing the
- 446 differentiation of mesenchymal stem cells. *Proceedings of the National Academy of*
- 447 *Sciences*, **107(11)**, pp.4872-4877.
- 448 28. Albert, P. and Schwarz, U., 2014. Dynamics of Cell Shape and Forces on Micropatterned
- 449 Substrates Predicted by a Cellular Potts Model. *Biophysical Journal*, **106(11)**, pp.2340-
- 450 2352.
- 451 29. Théry, M., Pépin, A., Dressaire, E., Chen, Y. and Bornens, M., 2006. Cell distribution of
- 452 stress fibres in response to the geometry of the adhesive environment. *Cell Motility and*
- 453 *the Cytoskeleton*, **63(6)**, pp.341-355.
- 454 30. Oakes, P.W., Banerjee, S., Marchetti, M.C. and Gardel, M.L., 2014. Geometry regulates
- 455 traction stresses in adherent cells. *Biophysical journal*, **107(4)**, pp.825-833.
- 456 31. Koushki, N., Ghagre, A., Srivastava, L.K., Sitaras, C., Yoshie, H., Molter, C. and Ehrlicher,
- 457 A., 2020. Lamin A redistribution mediated by nuclear deformation determines dynamic

458            localization of YAP. bioRxiv.  
459            32. Ruiz, S.A. and Chen, C.S., 2007. Microcontact printing: A tool to pattern. *Soft Matter*,  
460            **3(2)**, pp.168-177.